In-situ HRTEM observations of intermediate phase transformation in lattice reorientation in HCP rhenium

Yang He [a], Zhengwu Fang [a], Bin Li [b,*], Chongmin Wang [c,*], Scott X. Mao [a,*]

[a] Department of Mechanical Engineering and Materials Science, University of Pittsburgh, Pittsburgh, Pennsylvania 15261, USA

[b] Department of Industrial and Manufacturing Systems Engineering, Iowa State University, Ames, IA 50011, USA

[c] Environmental Molecular Sciences Laboratory, Pacific Northwest National Laboratory, Richland, Washington 99352, USA

* Corresponding authors: Scott X. Mao (sxm2@pitt.edu), Chongmin Wang (chongmin.wang@pnnl.gov), Bin Li (binl@iastate.edu).

Abstract

High resolution transmission electron microscopy (HRTEM) is performed to observe deformation behavior of hexagonal close-packed rhenium (Re) which is compressed along the $\langle 1\bar{1}00\rangle$ direction. Two types of lattice reorientation are observed during deformation. The first type involves the reorientation of one lattice by ~90° around $\langle 11\bar{2}0\rangle$, which is accomplished by the formation of an intermediate face-center-cubic (FCC) phase at the interface. This transformation sequence can be described as $\{1\bar{1}00\}_{matrix} \rightarrow \{111\}_{FCC} \rightarrow (0001)_{twin}$. In the second type, a new grain is formed but does not satisfy any known twin relationship with the matrix, and an intermediate FCC phase is also involved. The transformation sequence can be described as $\{1\bar{1}01\}_{matrix} \rightarrow \{111\}_{FCC} \rightarrow (0001)_{grain}$. Mechanisms responsible for the observed lattice reorientation and sequential phase transitions are analyzed by conducting lattice

correspondence analyses. Strain accommodation is also analyzed to explain the lattice reorientation and the intermediate phase transformations. The results provide new insight on the deformation mechanisms of HCP metals.

Key Words: Lattice Reorientation; Phase Transformation; Lattice Correspondence

1. Introduction

Formation of new grains can occur in crystalline materials as a result of plastic deformation or thermomechanical processing. When new grains are nucleated, how they select their orientation relationship (OR) with respect to the matrix and how grain boundaries (GBs) are formed and migrate remain a fundamental problem in materials science and engineering. Change in lattice reorientation can be produced by dislocation slip which involves high density dislocations, deformation twinning which efficiently reorients the lattice generally via glide of twinning dislocations, and GB activities including GB diffusion, GB migration [1], and climbing of GB dislocations [2]. For materials with nanograins, lattice reorientation typically occurs as a result of GB activities and plays a critical role in their mechanical properties and microstructure evolution [2–5]. For coarse-grained metallic materials, new grains are nucleated as a result of dynamic recrystallization that leads to texture development during processing [6–8], which strongly affects the mechanical properties of materials. Therefore, it is of great interest to resolve the fundamental mechanisms for lattice reorientation in crystalline materials.

Recently, abnormal lattice reorientation phenomena have been reported in hexagonal close-packed (HCP) metals. For instance, Liu et al. [9] observed twinning-like lattice reorientation involving nucleation and migration of $(0001) \parallel \{1\bar{1}00\}$ or B∥P interface during deformation of HCP magnesium (Mg) submicron specimens. In this particular case, the OR between the matrix and the product lattice is close to the $\{10\bar{1}2\}\langle\bar{1}011\rangle$ twinning mode, but the interface entirely deviates from the $\{10\bar{1}2\}$ plane. Kou et al. [10] observed formation of a new grain at the crack tip of pure titanium. The matrix and the new grain do not satisfy any known twin relationship, but a special OR was identified: $(0001)_{matrix} \parallel (0\bar{1}11)_{grain}$, suggesting that an interface between (0001) and $(0\bar{1}11)$ has a finite mobility. Most recently, Liu et al. [11] conducted *in-situ* TEM

observations of c-axis compression of single crystal Mg at room temperature. They found that following the dislocation-mediated plastic deformation, new grains quickly formed and post-mortem HRTEM revealed that many GBs satisfied the $(0001)_{matrix} \parallel (10\bar{1}1)_{grain}$ OR. This type of GB was called Py‖B. Formation of new grains that are not in any twin relationship with the matrix was also observed during room temperature compression of both single-crystal [12] and polycrystalline [13] HCP Mg, but the nucleation and growth processes that account for the room temperature dynamic recrystallization remain unclear.

Atomistic simulations also showed that during lattice reorientation in Mg and Ti, intermediate phase transformations may occur [14–16]. A metastable phase forms at the interface, assisting the matrix lattice to reorient toward the product lattice. Intermediate HCP → FCC or HCP → BCC phase transition occurred at extremely incoherent twin boundaries that entirely deviate from the $\{10\bar{1}2\}$ twinning plane. This behavior is similar to the lattice reorientation in body-centered cubic (BCC) metals that is mediated by the formation of a face-centered cubic (FCC) phase [17,18]. These simulation studies indicate that intermediate or sequential phase transitions could be an important mechanism for nucleation and growth of new grains during deformation and processing. However, so far, no *in-situ* experimental observations on the atomic scale have been reported.

The purpose of the present work is to perform *in-situ* high-resolution transmission electron microscopy (HRTEM) and directly observe lattice reorientation in HCP single crystal rhenium (Re) during deformation. Specifically, sequential phase transitions are uncovered during $\langle 1\bar{1}00\rangle$ compressive loading that favors $\{10\bar{1}2\}\langle\bar{1}011\rangle$ twinning. Atomistic simulations are also conducted to better understand the mechanisms that account for the experimentally observed phase transitions. The results obtained provide new insight on phase transition facilitated plastic deformation in HCP metals.

2. Experimental and simulation method

HCP Re is used for the *in-situ* HRTEM studies in this work. To conduct such experiments, a specimen must have superb resistance to oxidation because oxide film on the specimen surfaces would thwart the effort of acquiring atomic resolution images. Re has superior ductility and resistance to oxidation and electron beam (EB) damage in TEM [19], making Re a perfect candidate for our *in-situ* HRTEM experiments. Additionally, as a refractory metal, Re has important applications as structural components in ultra-high temperature environment [20,21].

Re nanocrystals are first fabricated from Re rods with 99.999% purity. Details of fabrication using focused ion beam (FIB) can be found in [22]. Then, the Re nanocrystals are loaded on both fixed-side and piezo-side of a Nanofactory STM (Scanning Tunnelling Microscopy) holder which is then inserted into the TEM chamber. FEI Titan 80-300 ETEM with imaging lens Cs corrector is used for our experiments and the operating voltage is 300 *keV*. The Re nanopillar on the piezo-side is driven with a high precision by the piezo-system toward the Re nanopillar on the fixed-side until they are in contact. Then, an electric pulse is applied to weld the two crystals together, forming a bi-crystal setting in which the crystal on the piezo-side acts as an indenter. Compression is applied by using the piezo-system at a controlled strain rate of $\sim 10^{-3}$ s^{-1}. Two settings are designed for our experiments. In the first setting (Fig. 1a), the bi-crystal is oriented such that their *c*-axes are perpendicular to each other and the zone axis is along the $\langle 11\bar{2}0\rangle$, i.e., the two crystals are close to the $\{10\bar{1}2\}\langle 10\bar{1}\bar{1}\rangle$ twin relationship. In the second setting (Fig. 1b), the crystal on the fixed-side is oriented such that the EB is along the $\langle 2\bar{1}\bar{1}3\rangle$ and the loading direction is along the $\langle 01\bar{1}0\rangle$. This crystal has an hour-glass shape. Real-time videos are recorded with a charge-coupled device (CCD) at ~2 frames per second.

To better understand the deformation mechanisms, we also conduct atomistic simulations. The starting configurations of our simulations are shown in Fig. 2. The orientations of the crystals in the simulations are identical to that of the experiments. In Fig. 2a, a bi-crystal is constructed such that the *c*-axes are perpendicular to each other, and the GB falls between the prismatic plane of top crystal and the basal plane of bottom crystal. The bi-crystal contains ~1.32 million atoms. A prismatic plane (colored in light blue) and a basal plane (in yellow) of the top crystal are pre-selected to analyze the lattice transformation. Such an analysis is critical to reveal how a lattice is transformed into the other during deformation and what processes (shear and/or shuffle) are involved. In Fig. 2b, an hour-glass single crystal is constructed to simulate the stress state of the deformed crystal in the experiments. The orientation of the single crystal is the same as the deformed crystal in the experiments, i.e., the viewing direction is along the $[2\bar{1}\bar{1}3]$ and the vertical direction is along the $[01\bar{1}0]$. The system contains about 1.3 million atoms. Large-scale Atomic/Molecular Massively Parallel Simulator (LAMMPS) [23,24] is used for the present work. In both simulations, a compressive strain is generated by pushing upward those atoms on the bottom surface at a constant displacement rate while atoms on the top surface are fixed. The displacement rate produces a strain rate of $\sim 10^8\ s^{-1}$. The temperature of both simulations is fixed at 300 K during compressive loading by applying the Nosé-Hoover [25,26] thermostat. No periodic boundary condition is applied. The time step size equals 1.0 *fs*. To identify different crystal structures generated in our simulations, common neighbor analysis [27] is used to differentiate and color the phases, and this is done with the visualizing package OVITO [28].

3. Results and analyses

3.1 In-situ HRTEM observations

We first present the in-situ HRTEM results, then these results are compared with the atomistic simulations. Fig. 3 shows snapshots, in time sequence, of the growth of an FCC phase sandwiched between the top (matrix) and bottom crystal (twin). As shown in Fig. 1a, the wedge-shaped FCC emerges on both sides where the interface intersects the left and right surface. At this magnified view (Fig. 3a), it can be seen that the orientation relationship (OR) between the matrix and the FCC satisfies: $(111)_{FCC} \parallel (1\bar{1}00)_{matrix}$, $[11\bar{2}]_{FCC} \parallel [0001]_{matrix}$; and the OR between the FCC and the twin satisfies: $(111)_{FCC} \parallel (0001)_{twin}$, $[11\bar{2}]_{FCC} \parallel [1\bar{1}00]_{G1}$. One-layer steps can be resolved at the FCC-Matrix interface. These steps shift as indicated by the arrows when the FCC grows into the matrix. As the shear strain increases, the FCC expands (Fig. 3b), as denoted by the blue lines (current interface position). For comparison, the previous interface position is also shown by the dotted green lines. A shear displacement can be seen along the $[11\bar{2}]$ of FCC. Fig. 3c is a magnified view of the interface region between the matrix and the FCC. This image contains important information about how the HCP matrix is transformed into the FCC during deformation. Two processes are required to accomplish the lattice transformation. The first is atomic shuffles. As shown in Fig. 3c, a prismatic plan has a corrugated, double-layered structure, as indicated by the green lines across the atoms on the prismatic plane. To transform the double-layered prismatic plane into a single-layered (111) plane of FCC, shuffles along the vertical direction are needed. However, this double-layer to single-layer transformation via shuffling does not produce the correct FCC stacking. Thus, an in-plane shear is also required, and this displacement vector is defined by the Burgers circuit (Fig. 3c). As such, the shuffles and the in-plane shear transform the HCP lattice of matrix into the FCC lattice. The magnitude of this in-plane shear displacement is about 0.8 Å, corresponding to a shear strain ~0.34 which equals the ratio between the shear

displacement and the interplanar spacing. This agrees well with the shear strain derived from the 20° angle produced on the free surface (Fig. 3b).

The FCC phase is only metastable. As the strain increases, it gradually transforms back to HCP, however, toward the twin lattice which is the stable phase. Fig. 4a shows the wedge-shaped FCC at a time point. After 10 seconds, the FCC moves upward, but a slab of FCC region is left behind and embedded inside the HCP twin (Fig. 4b). The FCC slab is formed when the wedge-shaped FCC regions on both sides expand laterally and eventually connect. Then the FCC slab is transformed into the HCP twin (Fig. 4c). These *in-situ* HRTEM observations indicate that the HCP → FCC transformation is an intermediate process between the HCP matrix and the twin.

Similar HCP → FCC transformation is also observed in the second experimental setting when an hour-glass shaped crystal is compressed along the $[1\bar{1}00]$. The result is shown in Fig. 5. Compression in this direction also favors $\{10\bar{1}2\}$ twinning. It can be seen the middle section of the specimen has been twinned. Above the twinned region is an FCC zone. Interestingly, a new triangular region is also formed, as indicated by the brown box. Careful examination shows that this is neither a $\{10\bar{1}2\}$ twin nor other type of twin, but a new grain that has a special OR with the matrix.

To show the structural evolution and the OR of the new grain, we present snapshots in time sequence in Fig. 6. The untransformed, initial HCP matrix is shown in Fig. 6a. After 11 seconds, the new grain is nucleated. However, inside this grain, an FCC structure at the bottom can be resolved (Fig. 6b). The top triangular region is a mixture of both FCC and HCP, and this becomes clear in Fig. 6c as the strain increases. The HCP matrix is first transformed into FCC which has a different orientation from the FCC at the bottom. Then an HCP is formed inside the FCC. Eventually, the HCP grows at the expense of the FCC. However, the FCC at the bottom remains.

To reveal the OR between the FCC, new HCP in the new grain and the HCP matrix, a magnified view is shown in Fig. 7. It can be seen that the OR between the FCC and the matrix is such that $(111)_{FCC} \parallel (\bar{1}101)_{matrix}$. The OR between the HCP new grain and the matrix satisfies $(0001)_{G2} \parallel (\bar{1}101)_{matrix}$, but this OR does not satisfy any known twin relationship. The OR between the FCC and HCP in the new grain is the same as that in Fig. 3, i.e., $(111)_{FCC} \parallel (0001)_{G2}$.

3.2 Simulation results

When the bi-crystal that satisfies $\{10\bar{1}2\}$ twin relationship is compressed along the $[1\bar{1}00]$ of the top crystal, HCP → FCC transformation is indeed well reproduced in our simulation. Fig. 8 shows a snapshot of a cross-sectional view of the system. A thin slice (0.5 nm) is taken out of the system along the viewing direction $[11\bar{2}0]$. Several important features can be observed. Two wedge-shaped FCC regions are formed, which is consistent with the *in-situ* HRTEM observations (Fig. 1a and Fig. 3). The lattice correspondence can now be clearly resolved. The pre-selected $(1\bar{1}00)$ prismatic plane (in light blue) has been transformed into the (111) of FCC which is a flat, single-layered plane. These two corresponding planes remain nearly parallel to each other during phase transformation, indicating that no homogeneous shear has occurred on the HCP-FCC interface which consists of multiple one-layer steps (see Fig. 9 below). The length of the steps is on the order of ~1.0 nm. The structure of the interface will be analyzed below. Meanwhile, the pre-selected (0001) basal plane (in yellow) has been transformed into the $(11\bar{1})$ of FCC. Then the $(11\bar{1})$ of FCC is transformed to the $(1\bar{1}00)$ of the twin (bottom crystal). This reverse transformation is accomplished by Shockley partial dislocations that erase the retained FCC layer by layer. This is also well consistent with our experimental observations in Fig. 4. The overall lattice transformation can be described as: $(1\bar{1}00)_{matrix} \rightarrow (111)_{FCC} \rightarrow (0001)_{twin}$, and $(0001)_{matrix} \rightarrow (11\bar{1})_{FCC} \rightarrow (1\bar{1}00)_{twin}$. If the intermediate phase transformation is ignored, the

net lattice transformation is simply the prismatic ↔ basal mutual transformation, which is exactly the mechanism for $\{10\bar{1}2\}$ twinning in HCP structures.

Uniaxial compression of the hour-glass shaped single crystal in our atomistic simulations is also consistent with the in-situ HRTEM observation. Fig. 10a shows that, during compression, a new grain (G1) is nucleated at the surface and grows into the matrix. Inside G1, an FCC structure can be seen (in green). The grain boundaries appear to be incoherent. To analyze the OR between G1 and the matrix, a thin slice (the boxed region) is taken out and tilted to a zone axis (see Fig. 11 below). As the strain increases, another grain G2 is also nucleated from the opposite surface of the narrowest section of the single crystal. Meanwhile, multiple $\{10\bar{1}1\}$ and $\{10\bar{1}2\}$ twins are nucleated. Inside the $\{10\bar{1}2\}$ twin and the new grains G1 and G2, FCC regions can be observed. But eventually, the FCC regions are transformed back to HCP in the new grains and the twins. Similarly, this reverse transformation is accomplished by nucleation and glide of Shockley partial dislocations that erase the FCC.

Fig. 11 shows the magnified view of the boxed region in Fig. 10a. The thin slice is tilted such that the viewing direction is along the zone axis of $\langle 1\bar{2}10\rangle$. The new grain G1 is enclosed by the blue atoms that are located between the matrix and grain G1. It is clear that the OR between the matrix and the FCC satisfies: $(111)_{FCC} \parallel \{10\bar{1}1\}_M$, $[11\bar{2}]_{FCC} \parallel \langle 10\bar{1}2\rangle_M$. The OR between the matrix and the new grain G1 satisfies: $(0001)_{G1} \parallel \{10\bar{1}1\}_M$, $\langle 10\bar{1}0\rangle_{FCC} \parallel \langle 10\bar{1}2\rangle_M$. It is worth noting that this OR does not satisfy any known twin relationship in HCP metals.

4. Discussion

Our *in-situ* HRTEM observations and atomistic simulations uncover two different pathways of deformation graining via intermediate phase transformation during compression of single

crystal Re, leading to the formation of new grains that have special ORs with the matrix. Intermediate phase transition from HCP to FCC occurs first, then the FCC is transformed back to HCP which orients differently from the initial matrix. In the literature reports, several pathways of HCP → FCC transformation have been identified in HCP metals [29–32]. The most commonly observed OR between HCP and FCC is: $(0001)_{HCP} \parallel (111)_{FCC}$, $[1\bar{1}00]_{HCP} \parallel [11\bar{2}]_{FCC}$, and $[11\bar{2}0]_{HCP} \parallel [\bar{1}10]_{FCC}$. This pathway is essentially the same as the second step of FCC → HCP transformation observed in our experiments and simulations, and this OR is the classical one that involves Shockley partials in the transformation.

Experimental results in the literature suggest that the HCP → FCC transformation is mediated by Shockley partial dislocations gliding on every other basal planes [33–35] or by mixed partial dislocations dissociated from both screw and 60°$\langle a \rangle$ dislocations on HCP basal planes [32]. Both mechanisms are essentially the same in terms of transforming the close-packed basal planes of HCP into the close-packed $\{111\}$ planes of FCC. Another HCP → FCC pathway was inferred based on the OR $(1\bar{1}00)_{HCP} \parallel (1\bar{1}0)_{FCC}$, $[0001]_{HCP} \parallel [002]_{FCC}$, $[11\bar{2}0]_{HCP} \parallel [110]_{FCC}$ that is often found in titanium after severe plastic deformation [31,36]. In this pathway, the $\{1\bar{1}00\}$ prismatic plane of HCP is transformed to the $\{1\bar{1}0\}$ plane of FCC.

In our work, the observed two HCP → FCC pathways differ from the abovementioned ones. An FCC structure emerges as an intermediate phase in the sequential HCP → FCC → HCP transformations that lead to the formation of new grains and change of orientation of the matrix. Thermodynamically, the FCC is not the equilibrium phase at the simulation temperature. We calculate the energy of FCC and HCP Re using the EAM potential and first principles. Our first principles calculations show that the ground state energy of HCP Re is ~60 meV/atom lower than FCC Re. With the EAM potential for Re, HCP Re is ~20 meV/atom lower than FCC Re. These

calculations indicate that the HCP is the equilibrium phase and the FCC is not energetically favorable. Thus, the presence of FCC is a result of strain accommodation. In the following, we discuss how and why the two HCP → FCC pathways occur in our experiments and simulations.

4.1 Lattice correspondence in deformation graining and phase transformation

Martensitic transformations and deformation twinning are important modes in mechanical properties of materials, especially those with limited dislocation sources or loaded under extreme conditions [37,38]. What interfacial defects mediate migration of interphase boundaries and twin boundaries have been discussed extensively [39–41]. Among the theories, disconnections [41] have been proposed to account for the migration of nearly all kinds of twin boundaries, interphase boundaries and grain boundaries. However, the way disconnections were defined cannot correctly describe the lattice correspondence in migration of interfaces in solid-state transformations whose mechanisms are far more complicated.

As shown in our *in-situ* HRTEM observations and atomistic simulations, lattice transformations between certain pairs of crystallographic planes can take place more easily than others. Accordingly, interfaces between these atomic planes have a high mobility. For a typical example, in $\{10\bar{1}2\}\langle\bar{1}011\rangle$ twinning, which is the most important twinning mode in HCP structures, the lattice transformation or lattice correspondence is such that the parent basal is transformed into the twin prismatic, and the parent prismatic is transformed into the twin basal. Thus, the basal and the prismatic are a pair of corresponding planes. This lattice transformation, which can be described as $(0002)_{matrix} \rightarrow (10\bar{1}0)_{twin}$, and $(10\bar{1}0)_{matrix} \rightarrow (0002)_{twin}$, has been observed extensively HCP metals both in experiments and simulations [9,22,42–45]. This is one of the manifestations of the important principle in solid-state transformations including martensitic transformations, deformation twinning and GB migration: an atomic plane of the

parent lattice must be transformed into its corresponding plane of the product lattice. As such, a strict one-to-one lattice correspondence or lattice transformation exists between the parent and the product phase [37]. Therefore, it is crucial to examine the lattice correspondence between the HCP and FCC such that structurally favorable transformation pathways can be identified.

The one-to-one lattice correspondence in various twinning modes of different crystal structures can be inferred mathematically by assuming two invariant planes that must be undistorted during twin boundary migration. A correspondence tensor $\boldsymbol{C}$, which is a second rank tensor, can be inferred by taking into consideration the deformation gradient tensor which is defined by the homogeneous twinning shear, and the coordinate transformation tensors between the parent and the product lattice which can be obtained from the well-defined OR [37,46]. Any vector $\boldsymbol{u}$ of the parent is transformed to a corresponding vector $\boldsymbol{v}$ by $\boldsymbol{v} = \boldsymbol{C} \cdot \boldsymbol{u}$. Naturally, this transformation is also applicable to any atomic planes. The correspondence tensors for the major twinning modes in HCP metals were derived by Niewczas [47], and the corresponding planes and vectors of various slip systems were inferred. For the most important $\{10\bar{1}2\}$ mode, it is seen that indeed, the corresponding plane of parent basal (0001) is exactly the twin prismatic $\{1\bar{1}00\}$. This explains well why interfaces between (0001) and $\{1\bar{1}00\}$, or the so-called B‖P or P‖B interfaces are very commonly observed in experiments and simulations. At the early stage of dynamic recrystallization of Mg, formation of this type of interface plays an important role in nucleation and growth of new grains [8]. However, it should be noted that the theoretical twinning plane $\{10\bar{1}2\}$ is not an invariant plane, as pointed out by Li and Zhang [44]. Despite this, the lattice correspondence still holds, although a homogenous shear cannot occur on the $\{10\bar{1}2\}$ twinning plane. In migration of some symmetric tilt grain boundaries by shear coupling [48], the GB plane is only partially invariant [49], but a lattice transformation can still be defined, and very complex

atomic shuffles are required. In the HCP → FCC transformation via $(1\bar{1}00)_{matrix} \rightarrow (111)_{FCC}$ (Fig. 3 and Fig. 8-9), the HCP and FCC are both close-packed. The atomic structure of a (111) of FCC is essentially the same as a (0001) of HCP. Thus, a $\{1\bar{1}00\}$ prismatic plane can transform to a (111) of FCC as easily as to the (0001) of HCP. However, the shuffles that transform a double-layered $\{1\bar{1}00\}$ into a single-layered (111) alone cannot create the correct FCC stacking. As shown in Fig. 3c and Fig. 9, an in-plane shear is needed such that the (0001) of HCP matrix is transformed into the $(11\bar{1})$ of FCC. It is important to note that this is not the "invariant plane" shear defined in the classical theory for martensitic transformation. In Fig. 9, the interface between the HCP matrix and the FCC is composed of nanoscale one-layer steps, indicating the invariant plane strain condition does not hold. This can also be seen from the fact that, if there were a homogeneous shear on the HCP-FCC interface, the pre-selected blue and the yellow plane should experience the same homogeneous shear, but obviously this is not the case because the blue plane undergoes almost zero shear whereas the yellow plane undergoes a fairly large shear. Thus, actually there is no homogeneous shear on the HCP-FCC interface.

From the calculation results by Niewczas [47] and the simulation by Li and Ma [50], $\{10\bar{1}\bar{1}\}$ and (0001) are exactly a pair of corresponding planes in $\{10\bar{1}1\}\langle 10\bar{1}\bar{2}\rangle$ twinning mode which has also been frequently observed in HCP metals [51–53]. For those HCP metals with a *c*/*a* ratio less than $\sqrt{3}$, this twinning mode is favored when a compressive load is applied along the *c*-axis of a crystal, and it is oftentimes called "contraction twinning" [54]. During twin boundary migration, the (0001) basal plane of parent is transformed into the $\{10\bar{1}\bar{1}\}$ pyramidal plane of twin, and the $\{10\bar{1}\bar{1}\}$ of parent is transformed into the (0001) of twin. Because the $\{10\bar{1}1\}$ and (0001) are a pair of corresponding planes, when a GB is formed between these two planes, the GB has a finite mobility even at room temperature. The migration of such grain boundaries also involves no

dislocations and only atomic shuffles are involved. Most recently, Li and Chen [55] observed intermediate FCC → HCP → FCC sequential phase transformations in migration of symmetric tilt grain boundaries in Cu and Ni but not in Al. By forming an intermediate HCP at the grain boundaries, the mobility of the original grain boundaries was enhanced due to the creation of mobile $(111)_{FCC} \parallel (0002)_{HCP}$ and $(111)_{FCC} \parallel \{10\bar{1}1\}_{HCP}$ interfaces. The mutual transformations between the $\{1\bar{1}00\}$, (0001) and $\{10\bar{1}1\}$ of HCP are illustrated below.

In theory, the magnitude of twinning shear for $\{10\bar{1}2\}\langle 10\bar{1}1\rangle$ and $\{10\bar{1}1\}\langle\bar{1}012\rangle$ in Re is $\frac{|\gamma^2-3|}{\gamma\sqrt{3}} \approx 0.14$ and $\frac{4\gamma^2-9}{4\gamma\sqrt{3}} \approx 0.13$, respectively [43], where γ is the c/a = 1.615 for Re. These small values of magnitude of twinning shear imply that complex atomic shuffles are required to complete the lattice transformation between parent and twin [39]. In Fig. 12, we plot the atomic structure of the $\{1\bar{1}00\}$, (0001) and $\{10\bar{1}1\}$ such that the viewing direction is along the respective plane normal. The plots are made in the same magnification with respect to the lattice parameter *a* and *c* so that direct dimensional comparison can be made. If we compare the structure of $\{1\bar{1}00\}$ and (0001), the atomic structure of these two planes is so close that only minor shuffles are needed to transform a $\{1\bar{1}00\}$ into a (0001), or vice versa. Note that other shuffles are needed to transform a double-layered prismatic into a single-layered basal. If we compare the atomic structure of a $\{10\bar{1}1\}$ pyramidal and a (0001) basal, relatively large shuffles ($\sim\frac{a}{2}$) roughly along the $\langle 11\bar{2}0\rangle$ direction (indicated by the green arrows and the dotted circles) are needed to transform a $\{10\bar{1}1\}$ into a (0001). Minor shuffles are also needed to transform a double-layered $\{10\bar{1}1\}$ into a single-layered (0001). Despite this, the structure of these two corresponding planes is still pretty close. Such a similarity in atomic structure between corresponding planes is implicitly prescribed in the classical twinning theory. Again, because the atomic structure of a (0001) basal is essentially the

same as a {111} of FCC, the transformation from HCP to FCC via the pathway $\{1\bar{1}01\}_{HCP} \rightarrow \{111\}_{FCC}$ can occur if stress condition is satisfied.

4.2 Strain accommodation via intermediate phase transformation

The deformation graining and the intermediate phase transition involved in the compression tests of single crystal Re must have occurred as mechanisms for strain accommodation. The lattice transformations provide deformation modes that are able to compensate the external strain. Additionally, in the case of nucleation of new grains that do not satisfy any twin relationship to the matrix, the formation of new grains (Fig. 10a) provides extra dislocation slip modes to better accommodate the plastic strain. This can be understood from the fact that, in the compression of the single crystals (Fig. 1b), basal slip is suppressed because the loading direction is either perpendicular or parallel to the basal normal, and these slip systems have close to zero Schmid factors. When a new grain is formed (Fig. 5), more easy slip systems can be activated. To demonstrate this point, we analyze the strains produced by the lattice transformations during deformation graining and the observed sequential phase transformations. As shown in Fig. 1a, the sequential transitions of $\{1\bar{1}00\}_{Matrix} \rightarrow \{111\}_{FCC} \rightarrow (0001)_{twin}$ generate a total of compressive strain of ~6.8% along the $[1\bar{1}00]$ direction of the matrix as a result of lattice reorientation. The interplanar spacing along this direction changes from $\frac{\sqrt{3}}{2}a \rightarrow \frac{\sqrt{6}}{3}a \rightarrow \frac{\gamma}{2}a$, (for Re, a = 0.276 nm). Therefore, the above sequential transformations effectively accommodate the external compressive strain along the $[1\bar{1}00]$ direction of the matrix. Moreover, it is noted that the $\{1\bar{1}00\}_{matrix} \rightarrow \{111\}_{FCC}$ and $\{111\}_{FCC} \rightarrow (0002)_{twin}$ transformations produce a local shear strain on the free surfaces (the shear magnitude is ~0.36) (Fig. 3c). Without this shear strain, a sharp straight angle step would be created on the free surfaces and a material discontinuity would occurred [16]. This is because there is a misfit strain between the matrix and the twin along the

[0001] direction of matrix (Fig. 12). This misfit strain equals $\frac{\sqrt{3}-\gamma}{\gamma} = 7.2\%$, indicating that an extension occurs along the [0001] direction of matrix whereas a contraction occurs along compression direction.

In comparison, the sequential $\{\bar{1}101\}_{matrix} \rightarrow \{111\}_{FCC} \rightarrow (0001)_{grain}$ transformations introduce a local shear strain roughly along the $\langle\bar{5}\ \bar{8}\ 13\ 2.876\rangle$ direction (nearly parallel to the $\langle 11\bar{2}\rangle$ direction of intermediate FCC phase and the $[1\bar{1}00]$ direction of the final HCP phase) on the $(1\bar{1}01)$ plane of the matrix (Fig. 11). The surface tilt of ~18° observed in Fig. 7 is in accordance with the theoretical shear angle for the $\{\bar{1}101\}_{matrix} \rightarrow \{111\}_{FCC}$ lattice transformation, which equals ~18°. Additionally, the $\{\bar{1}101\}_{matrix} \rightarrow \{111\}_{FCC}$ transformation also involves atomic shuffles that transforms the double-layered $\{\bar{1}101\}$ into the single-layered $\{111\}$ and this lattice transformation generates a contraction strain of ~5.5% roughly along the $[1\bar{1}02]$ direction of matrix: the dimensional difference equals $(\sqrt{3/4+\gamma^2}-\sqrt{3})a$ (Fig. 11).

Although the external loading condition in Fig. 1a is almost the same as that in Fig. 1b, i.e., compression along the $\langle 1\bar{1}00\rangle$ direction, the local stress/strain states should be different. Specifically, the sequential $\{\bar{1}101\}_{matrix)} \rightarrow \{111\}_{FCC} \rightarrow (0002)_{grain}$ transformation is activated at the surface of the narrowest section of the as-fabricated sample, where stress concentration can be expected. The resolved shear stress along the $(\bar{1}101)$ plane likely favors the nucleation of the new grains that have a $\{\bar{1}101\}_{matrix} \parallel \{111\}_{grain}$ orientation relationship with the matrix (Fig. 5), and the GB between these two atomic planes is mobile. Note that this particular mechanism can be reproduced in our atomistic simulations in which the shape of the single crystal mimics that of the experiment. The location of grain nucleation and the orientation relationship are all consistent, validating the mechanisms we propose.

The above intermediate phase transformations should also be applicable to other HCP metals such as Co [56], Hf [32], and Ti, since the emergence of metastable FCC phase has been observed during the plastic deformation of these metals. In addition, such transformations could also be activated at the stress-concentration areas in HCP bulk counterparts such as the intersection regions of grain boundaries [57] or phase variants [56], which could be an additional mechanism contributing to the room-temperature dynamic recrystallization in HCP metals [12,13]. Moreover, akin to the variant selection in deformation twinning [58], the lattice reorientation facilitated by the intermediate phase transformations in real cases may not be limited to the two types we have observed in this work. Instead, there could be other types of deformation graining processes that follow similar lattice correspondence relationships to what we have discussed, but may lead to different ORs, which warrants future investigations.

5. Conclusions

In this work, we conduct in-situ HRTEM observations of deformation behavior in HCP Re when compressed along the $\langle 1\bar{1}00\rangle$ direction. Lattice reorientation and intermediate phase transformation are captured. Atomistic simulations are also performed and the results are consistent with our experimental observations. The following conclusions can be drawn:

(1) Two sequential phase transitions are observed. The $\{1\bar{1}00\}_{matrix} \rightarrow \{111\}_{FCC} \rightarrow (0001)_{twin}$ transformations cause the matrix lattice to reorient by ~90° around the $\langle 11\bar{2}0\rangle$, which is close to $\{10\bar{1}2\}\langle 10\bar{1}\bar{1}\rangle$ twin relationship. The $\{1\bar{1}01\}_{matrix} \rightarrow \{111\}_{FCC} \rightarrow (0001)_{grain}$ transformations create a new grain that does not satisfy any known twin relationship with the matrix. The mechanisms behind these phase transitions can be well explained by the lattice correspondence principle implicitly prescribed in the classical theory of deformation twinning.

(2) Although the FCC Re is energetically unfavorable, the presence of FCC inside the new grain provides a strain accommodation under the loading conditions. Because the shuffling dominated lattice reorientation does not involve a homogeneous shear at the interface, the formation of an intermediate HCP phase provides additional shear modes that are needed for the plastic deformation.

Acknowledgements

S.X.M. acknowledges support from NSF CMMI 1536811 through University of Pittsburgh. C.M.W. was supported by PNNL LDRD program. B.L. thanks the support from NSF CMMI 1635088, 2016263 and 2032483. This work was performed, in part, at the William R. Wiley Environmental Molecular Sciences Laboratory, a national scientific user facility sponsored by U.S. Department of Energy, Office of Biological and Environmental Research and located at PNNL. PNNL is operated by Battelle for the U.S. Department of Energy under contract DE-AC05-76RLO1830.

References

[1] Q. Zhu, G. Cao, J. Wang, C. Deng, J. Li, Z. Zhang, S.X. Mao, In situ atomistic observation of disconnection-mediated grain boundary migration, Nat. Commun. 10 (2019) 156. https://doi.org/10.1038/s41467-018-08031-x.

[2] L. Wang, J. Teng, P. Liu, A. Hirata, E. Ma, Z. Zhang, M. Chen, X. Han, Grain rotation mediated by grain boundary dislocations in nanocrystalline platinum, Nat. Commun. 5 (2014) 4402. https://doi.org/10.1038/ncomms5402.

[3] Z. Shan, E.A. Stach, J.M.K. Wiezorek, J.A. Knapp, D.M. Follstaedt, S.X. Mao, Grain Boundary-Mediated Plasticity in Nanocrystalline Nickel, Science. 305 (2004) 654–657. https://doi.org/10.1126/science.1098741.

[4] J. Hu, Y.N. Shi, X. Sauvage, G. Sha, K. Lu, Grain boundary stability governs hardening and softening in extremely fine nanograined metals, Science. 355 (2017) 1292–1296. https://doi.org/10.1126/science.aal5166.

[5] D. Moldovan, V. Yamakov, D. Wolf, S.R. Phillpot, Scaling Behavior of Grain-Rotation-Induced Grain Growth, Phys. Rev. Lett. 89 (2002) 206101. https://doi.org/10.1103/PhysRevLett.89.206101.

[6] R.C. Gifkins, Grain-boundary sliding and its accommodation during creep and superplasticity, Metall. Trans. A. 7 (1976) 1225–1232. https://doi.org/10.1007/BF02656607.

[7] L. Jiang, J.J. Jonas, R.K. Mishra, A.A. Luo, A.K. Sachdev, S. Godet, Twinning and texture development in two Mg alloys subjected to loading along three different strain paths, Acta Mater. 55 (2007) 3899–3910. https://doi.org/10.1016/j.actamat.2007.03.006.

[8] Q. Ma, B. Li, E.B. Marin, S.J. Horstemeyer, Twinning-induced dynamic recrystallization in a magnesium alloy extruded at 450 °C, Scr. Mater. 65 (2011) 823–826. https://doi.org/10.1016/j.scriptamat.2011.07.046.

[9] B.-Y. Liu, J. Wang, B. Li, L. Lu, X.-Y. Zhang, Z.-W. Shan, J. Li, C.-L. Jia, J. Sun, E. Ma, Twinning-like lattice reorientation without a crystallographic twinning plane, Nat. Commun. 5 (2014). https://doi.org/10.1038/ncomms4297.

[10] Z. Kou, Y. Yang, L. Yang, B. Huang, X. Luo, In situ atomic-scale observation of a novel lattice reorienting process in pure Ti, Scr. Mater. 166 (2019) 144–148. https://doi.org/10.1016/j.scriptamat.2019.03.021.

[11] B.-Y. Liu, Z. Zhang, F. Liu, N. Yang, B. Li, P. Chen, Y. Wang, J.-H. Peng, J. Li, E. Ma, Z.-W. Shan, Rejuvenation of plasticity via deformation graining in magnesium, Nat. Commun. 13 (2022) 1060. https://doi.org/10.1038/s41467-022-28688-9.

[12] K.D. Molodov, T. Al-Samman, D.A. Molodov, G. Gottstein, Mechanisms of exceptional ductility of magnesium single crystal during deformation at room temperature: Multiple twinning and dynamic recrystallization, Acta Mater. 76 (2014) 314–330. https://doi.org/10.1016/j.actamat.2014.04.066.

[13] Z. Zeng, J.-F. Nie, S.-W. Xu, C. Davies, N. Birbilis, Super-formable pure magnesium at room temperature, Nat. Commun. 8 (2017) 972. https://doi.org/10.1038/s41467-017-01330-9.

[14] J. Ren, Q. Sun, L. Xiao, X. Ding, J. Sun, Phase transformation behavior in titanium single-crystal nanopillars under [0 0 0 1] orientation tension: A molecular dynamics simulation, Comput. Mater. Sci. 92 (2014) 8–12. https://doi.org/10.1016/j.commatsci.2014.05.018.

[15] J.P. Hirth, J. Wang, C.N. Tomé, Disconnections and other defects associated with twin interfaces, Prog. Mater. Sci. 83 (2016) 417–471. https://doi.org/10.1016/j.pmatsci.2016.07.003.

[16] P. Chen, F. Wang, B. Li, Transitory phase transformations during {10-12} twinning in titanium, Acta Mater. 171 (2019) 65–78. https://doi.org/10.1016/j.actamat.2019.04.002.

[17] Q. Wang, J. Wang, J. Li, Z. Zhang, S.X. Mao, Consecutive crystallographic reorientations and superplasticity in body-centered cubic niobium nanowires, Sci. Adv. 4 (2018) eaas8850. https://doi.org/10.1126/sciadv.aas8850.
[18] S.J. Wang, H. Wang, K. Du, W. Zhang, M.L. Sui, S.X. Mao, Deformation-induced structural transition in body-centred cubic molybdenum, Nat. Commun. 5 (2014) 3433. https://doi.org/10.1038/ncomms4433.
[19] R.F. Egerton, P. Li, M. Malac, Radiation damage in the TEM and SEM, Micron. 35 (2004) 399–409. https://doi.org/10.1016/j.micron.2004.02.003.
[20] J. Kacher, A.M. Minor, Twin boundary interactions with grain boundaries investigated in pure rhenium, Acta Mater. 81 (2014) 1–8. https://doi.org/10.1016/j.actamat.2014.08.013.
[21] J.-C. Carlen, B.D. Bryskin, Rhenium - A Unique Rare Metal, Mater. Manuf. Process. 9 (1994) 1087–1104. https://doi.org/10.1080/10426919408934977.
[22] Y. He, B. Li, C. Wang, S.X. Mao, Direct observation of dual-step twinning nucleation in hexagonal close-packed crystals, Nat. Commun. 11 (2020) 2483. https://doi.org/10.1038/s41467-020-16351-0.
[23] S. Plimpton, Fast Parallel Algorithms for Short-Range Molecular Dynamics, J. Comput. Phys. 117 (1995) 1–19. https://doi.org/10.1006/jcph.1995.1039.
[24] A.P. Thompson, H.M. Aktulga, R. Berger, D.S. Bolintineanu, W.M. Brown, P.S. Crozier, P.J. in 't Veld, A. Kohlmeyer, S.G. Moore, T.D. Nguyen, R. Shan, M.J. Stevens, J. Tranchida, C. Trott, S.J. Plimpton, LAMMPS - a flexible simulation tool for particle-based materials modeling at the atomic, meso, and continuum scales, Comput. Phys. Commun. 271 (2022) 108171. https://doi.org/10.1016/j.cpc.2021.108171.
[25] W.G. Hoover, Canonical dynamics: Equilibrium phase-space distributions, Phys. Rev. A. 31 (1985) 1695–1697. https://doi.org/10.1103/PhysRevA.31.1695.
[26] S. Nosé, A unified formulation of the constant temperature molecular dynamics methods, J. Chem. Phys. 81 (1984) 511–519. https://doi.org/10.1063/1.447334.
[27] J.Dana. Honeycutt, H.C. Andersen, Molecular dynamics study of melting and freezing of small Lennard-Jones clusters, J. Phys. Chem. 91 (1987) 4950–4963. https://doi.org/10.1021/j100303a014.
[28] A. Stukowski, Visualization and analysis of atomistic simulation data with OVITO–the Open Visualization Tool, Model. Simul. Mater. Sci. Eng. 18 (2009) 015012. https://doi.org/10.1088/0965-0393/18/1/015012.
[29] J.W. Christian, W. Hume-Rothery, A theory of the transformation in pure cobalt, Proc. R. Soc. Lond. Ser. Math. Phys. Sci. 206 (1997) 51–64. https://doi.org/10.1098/rspa.1951.0055.
[30] C. Hitzenberger, H.P. Karnthaler, Weak-beam TEM study of the h.c.p. to f.c.c. martensitic phase transformation lamellae in CoNi, Philos. Mag. A. 64 (1991) 151–163. https://doi.org/10.1080/01418619108206132.
[31] D.H. Hong, T.W. Lee, S.H. Lim, W.Y. Kim, S.K. Hwang, Stress-induced hexagonal close-packed to face-centered cubic phase transformation in commercial-purity titanium under cryogenic plane-strain compression, Scr. Mater. 69 (2013) 405–408. https://doi.org/10.1016/j.scriptamat.2013.05.038.
[32] H. Zhao, M. Song, S. Ni, S. Shao, J. Wang, X. Liao, Atomic-scale understanding of stress-induced phase transformation in cold-rolled Hf, Acta Mater. 131 (2017) 271–279. https://doi.org/10.1016/j.actamat.2017.03.058.
[33] Y. Liu, H. Yang, Y. Liu, B. Jiang, J. Ding, R. Woodward, Thermally induced fcc↔hcp martensitic transformation in Co–Ni, Acta Mater. 53 (2005) 3625–3634. https://doi.org/10.1016/j.actamat.2005.04.019.
[34] H. Yang, Y. Liu, Factors influencing the stress-induced fcc↔hcp martensitic transformation in Co–32Ni single crystal, Acta Mater. 54 (2006) 4895–4904. https://doi.org/10.1016/j.actamat.2006.06.047.

[35] T. Waitz, H.P. Karnthaler, The f.c.c. to h.c.p. martensitic phase transformation in CoNi studied by TEM and AFM methods, Acta Mater. 45 (1997) 837–847. https://doi.org/10.1016/S1359-6454(96)00184-X.
[36] H.C. Wu, A. Kumar, J. Wang, X.F. Bi, C.N. Tomé, Z. Zhang, S.X. Mao, Rolling-induced Face Centered Cubic Titanium in Hexagonal Close Packed Titanium at Room Temperature, Sci. Rep. 6 (2016) 24370. https://doi.org/10.1038/srep24370.
[37] J.W. Christian, The Theory of Transformations in Metals and Alloys, Newnes, 2002.
[38] Z.W. Shan, R.K. Mishra, S.A. Syed Asif, O.L. Warren, A.M. Minor, Mechanical annealing and source-limited deformation in submicrometre-diameter Ni crystals, Nat. Mater. 7 (2008) 115–119. https://doi.org/10.1038/nmat2085.
[39] J.W. Christian, S. Mahajan, Deformation twinning, Prog. Mater. Sci. 39 (1995) 1–157. https://doi.org/10.1016/0079-6425(94)00007-7.
[40] R.C. Pond, J.P. Hirth, Defects at Surfaces and Interfaces, in: H. Ehrenreich, D. Turnbull (Eds.), Solid State Phys., Academic Press, 1994: pp. 287–365. https://doi.org/10.1016/S0081-1947(08)60641-4.
[41] J.P. Hirth, R.C. Pond, Steps, dislocations and disconnections as interface defects relating to structure and phase transformations, Acta Mater. 44 (1996) 4749–4763. https://doi.org/10.1016/S1359-6454(96)00132-2.
[42] A. Luque, M. Ghazisaeidi, W.A. Curtin, Deformation modes in magnesium (0 0 0 1) and (0\,1\,\bar1\,1) single crystals: simulations versus experiments, Model. Simul. Mater. Sci. Eng. 21 (2013) 045010. https://doi.org/10.1088/0965-0393/21/4/045010.
[43] B. Xu, L. Capolungo, D. Rodney, On the importance of prismatic/basal interfaces in the growth of twins in hexagonal close packed crystals, Scr. Mater. 68 (2013) 901–904. https://doi.org/10.1016/j.scriptamat.2013.02.023.
[44] B. Li, X.Y. Zhang, Twinning with zero twinning shear, Scr. Mater. 125 (2016) 73–79. https://doi.org/10.1016/j.scriptamat.2016.07.004.
[45] B. Li, E. Ma, Atomic Shuffling Dominated Mechanism for Deformation Twinning in Magnesium, Phys. Rev. Lett. 103 (2009) 035503. https://doi.org/10.1103/PhysRevLett.103.035503.
[46] B.A. Bilby, A.G. Crocker, The Theory of the Crystallography of Deformation Twinning, Proc. R. Soc. Lond. Ser. Math. Phys. Sci. 288 (1965) 240–255. https://doi.org/10.1098/rspa.1965.0216.
[47] M. Niewczas, Lattice correspondence during twinning in hexagonal close-packed crystals, Acta Mater. 58 (2010) 5848–5857. https://doi.org/10.1016/j.actamat.2010.06.059.
[48] J.W. Cahn, Y. Mishin, A. Suzuki, Coupling grain boundary motion to shear deformation, Acta Mater. 54 (2006) 4953–4975. https://doi.org/10.1016/j.actamat.2006.08.004.
[49] B. Li, J. Leung, Lattice transformation in grain boundary migration via shear coupling and transition to sliding in face-centered-cubic copper, Acta Mater. 215 (2021) 117127. https://doi.org/10.1016/j.actamat.2021.117127.
[50] B. Li, E. Ma, Zonal dislocations mediating {10-11}<10-1-2> twinning in magnesium, Acta Mater. 57 (2009) 1734–1743. https://doi.org/10.1016/j.actamat.2008.12.016.
[51] I. Kim, J. Kim, D.H. Shin, X.Z. Liao, Y.T. Zhu, Deformation twins in pure titanium processed by equal channel angular pressing, Scr. Mater. 48 (2003) 813–817. https://doi.org/10.1016/S1359-6462(02)00513-4.
[52] Z. Kou, Y. Yang, B. Huang, X. Luo, P. Li, G. Zhao, W. Zhang, Observing the dynamic 101¯1 twining process in pure Ti at atomic resolution, Scr. Mater. 139 (2017) 139–143. https://doi.org/10.1016/j.scriptamat.2017.06.048.
[53] Y.M. Zhu, S.W. Xu, J.F. Nie, {101¯1} Twin boundary structures in a Mg–Gd alloy, Acta Mater. 143 (2018) 1–12. https://doi.org/10.1016/j.actamat.2017.09.067.
[54] M.H. Yoo, Interaction of Slip Dislocations with Twins in Hcp Metals, Trans. Metall. Soc. AIME. 245 (1969) 2051–2060.

[55] B. Li, K. Chen, Grain boundary migration facilitated by phase transformation and twinning in face-centered cubic metals, J. Mater. Sci. 58 (2023) 14740–14757. https://doi.org/10.1007/s10853-023-08863-z.
[56] R. Su, D. Neffati, J. Cho, Q. Li, J. Ding, H. Wang, Y. Kulkarni, X. Zhang, Phase transformation induced plasticity in high-strength hexagonal close packed Co with stacking faults, Scr. Mater. 173 (2019) 32–36. https://doi.org/10.1016/j.scriptamat.2019.07.030.
[57] S. Shekhar, A.H. King, Strain fields and energies of grain boundary triple junctions, Acta Mater. 56 (2008) 5728–5736. https://doi.org/10.1016/j.actamat.2008.07.053.
[58] Z.W. Huang, S.B. Jin, H. Zhou, Y.S. Li, Y. Cao, Y.T. Zhu, Evolution of twinning systems and variants during sequential twinning in cryo-rolled titanium, Int. J. Plast. 112 (2019) 52–67. https://doi.org/10.1016/j.ijplas.2018.08.008.

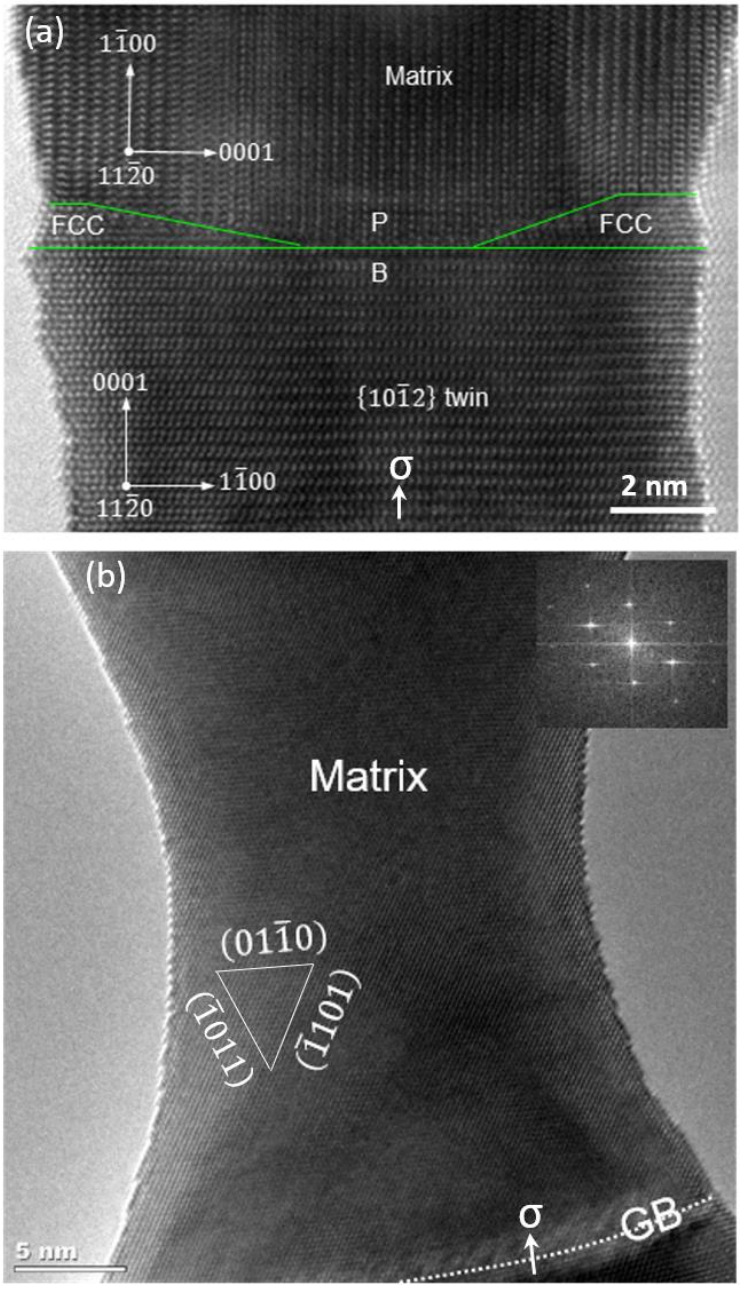

Fig. 1 In-situ HREM observation of deformation graining in HCP Re. (a) A bi-crystal is set up such that they satisfy $\{10\bar{1}2\}$ twin relationship. The zone axis is the $[11\bar{2}0]$. A compressive load is applied by pushing the bottom crystal upward. Note that an FCC phase is formed at the two regions where the interface intersects the surfaces. (b) Another bi-crystal is set up such that the viewing (electron beam) direction is along the $\langle 2\bar{1}\bar{1}3\rangle$. The top crystal has an hour-glass shape.

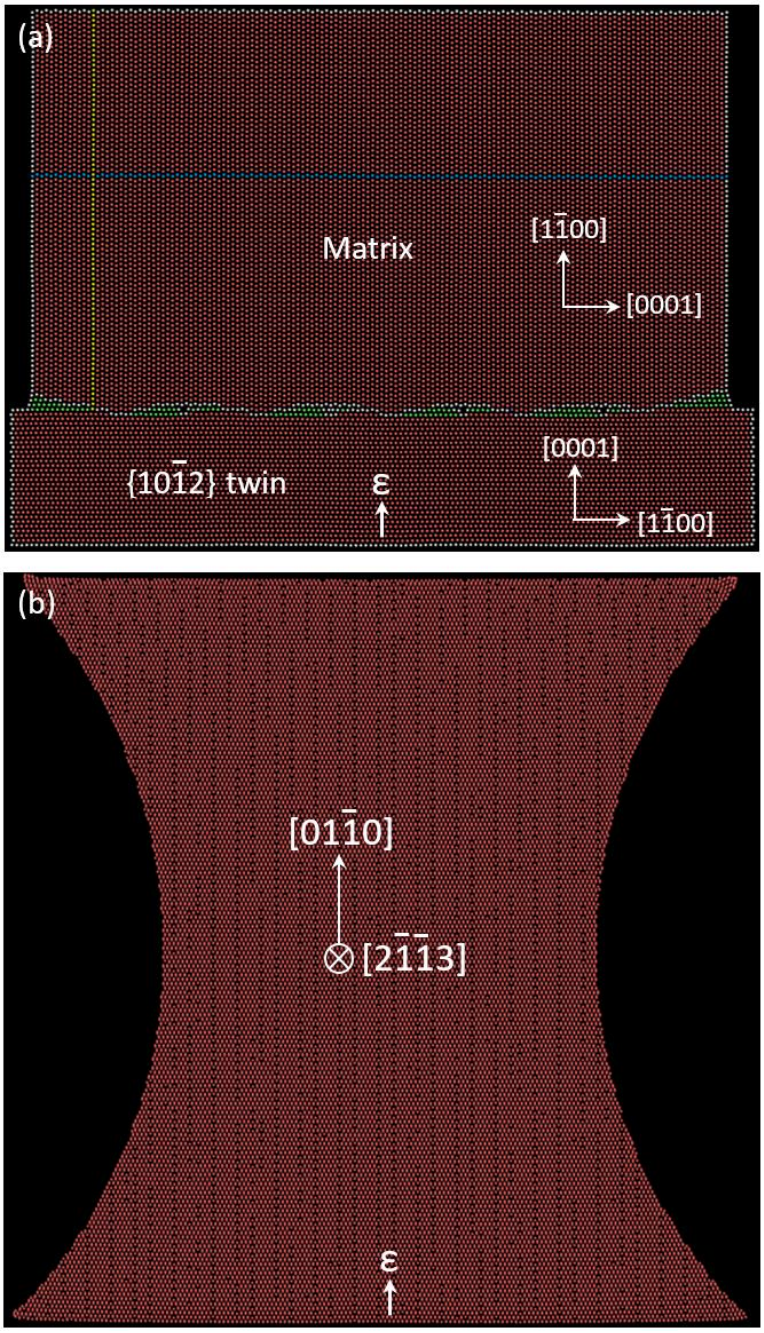

Fig. 2 (a) The initial set-up of a bi-crystal that satisfy $\{10\bar{1}2\}$ twin relationship in atomistic simulations. Zone axis $[11\bar{2}0]$. A basal plane (colored in yellow) and a prismatic plane of the matrix are pre-selected for lattice transformation analysis. (b) A single crystal that is oriented similarly to the in-situ HREM experiment in Fig. 1b. The crystal also has an hour-glass shape.

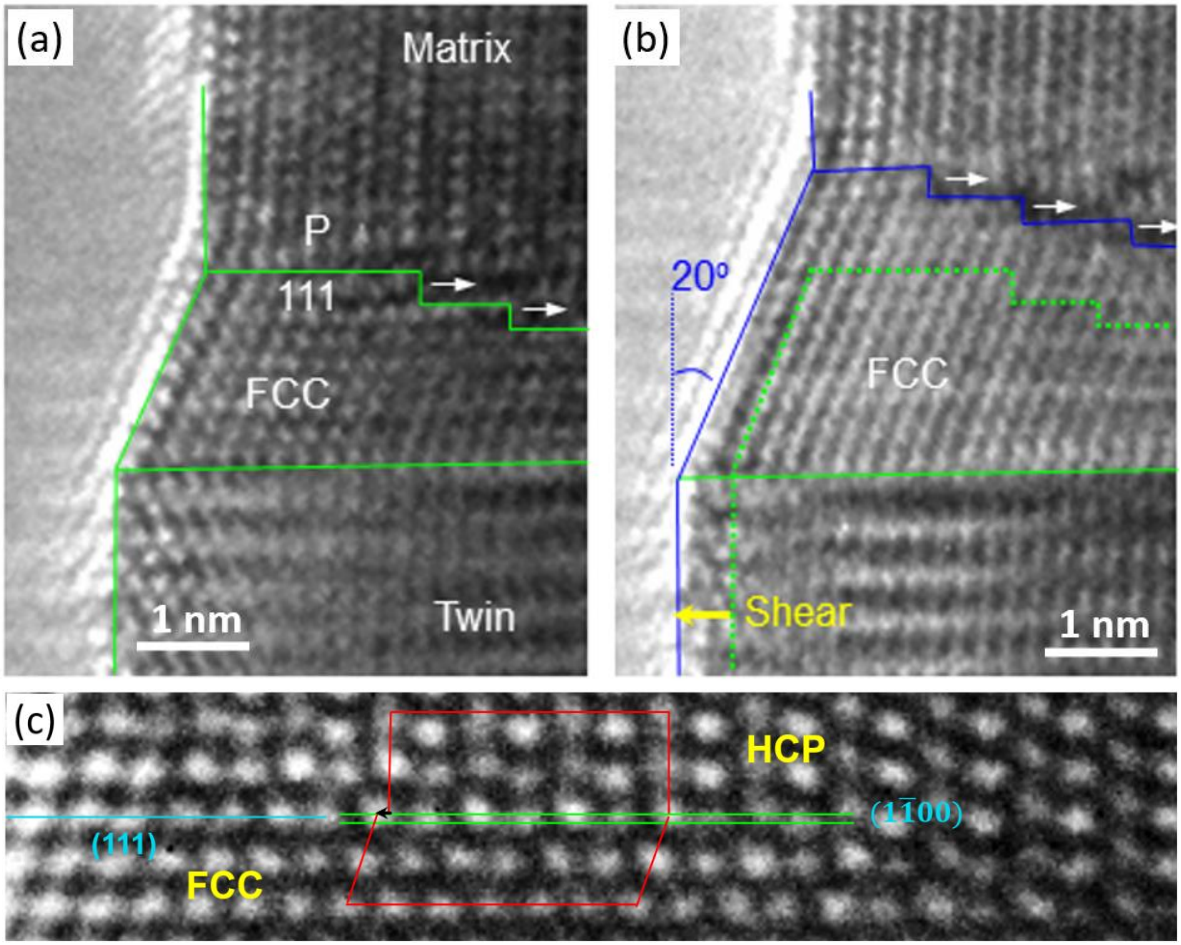

Fig. 3 HREM snapshots in time sequence showing the growth of FCC phase. (a) Steps are created at the top interface between the prismatic plane of HCP and the {111} plane of FCC. (b) The FCC region expands and grows into the HCP matrix. (c) Atomic resolution TEM image that reveals the transformation of the {1$\bar{1}$00} prismatic plane of matrix into the {111} plane of FCC. Two processes are involved: atomic shuffles that transform a corrugated prismatic plane of HCP into a flat {111} plane of FCC, and an in-plane shear that creates the correct stacking sequence of FCC, which is defined by the Burgers circuit.

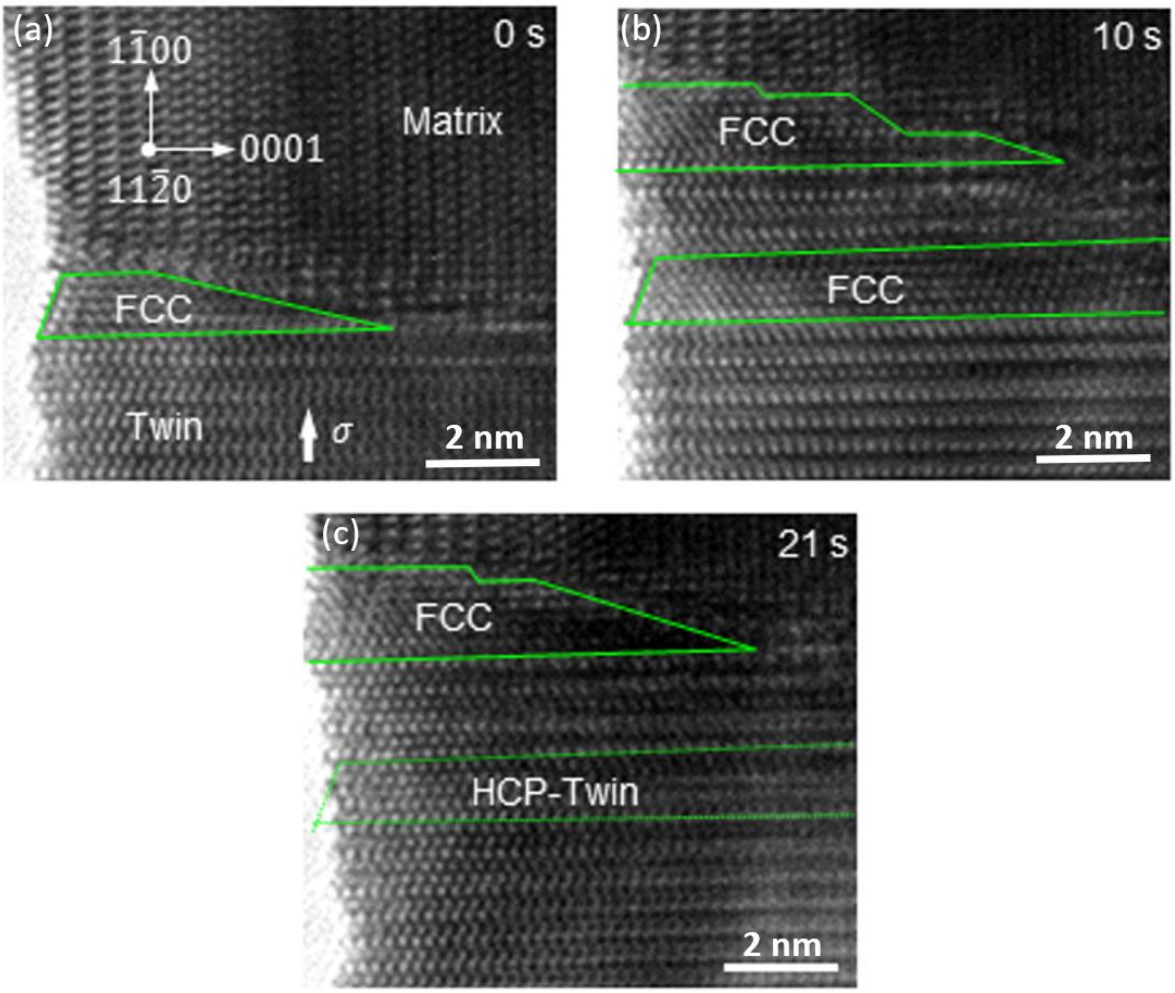

Fig. 4 Snapshots in time sequence of reverse transformation of the intermediate FCC into HCP twin. (a) HREM image of the FCC (enclosed by the green lines) sandwiched between the matrix and the twin. (b) The FCC region moves upward as the compressive strain increases, left behind is a slab of FCC embedded inside the HCP twin. (c) The FCC is transformed into the HCP twin. The FCC is an intermediate phase of the twinning process.

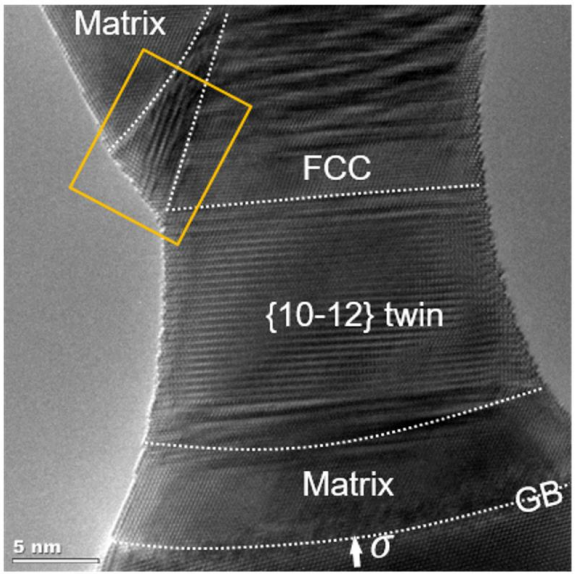

Fig. 5 Formation of a new grain (enclosed by the brown lines) when the crystal is compressed roughly along the $[1\bar{1}00]$ with the zone axis of $[2\bar{1}\bar{1}3]$. During compression, $\{10\bar{1}2\}$ twinning is activated. The twinned region is separated from the matrix by a layer of FCC phase. The new grain and the matrix do not satisfy any twin orientation relationship. The structural evolution of inside the new grain is shown in Fig. 6.

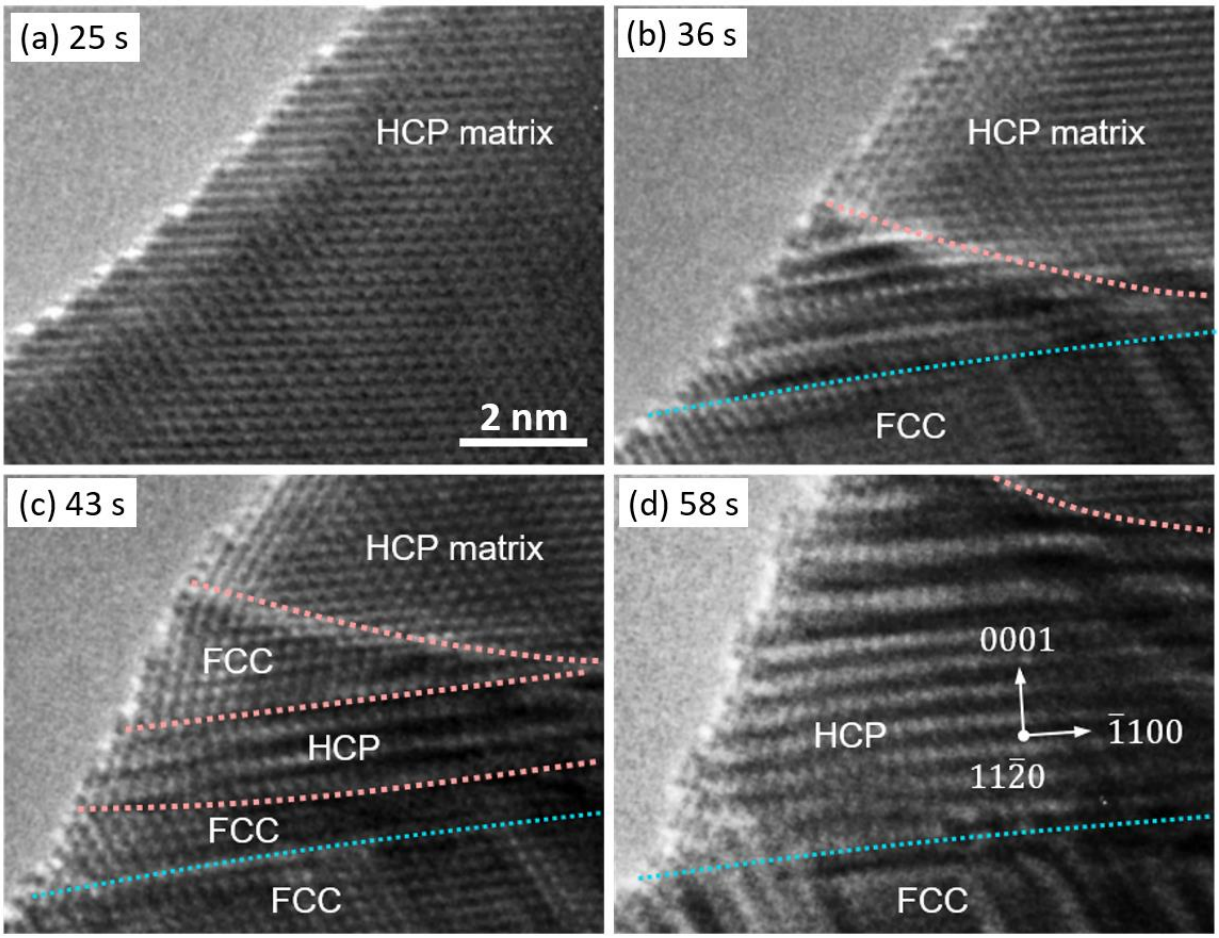

Fig. 6 HREM snapshots in time sequence showing the structural evolution inside the new grain. (a) The HCP matrix before the formation of the new grain. (b) As the new grain is nucleated, FCC phase is present inside the new grain. (c) As the strain increases, the FCC phase is transformed into HCP. (d) The HCP grows at the expense of the FCC. The new grain now contains both FCC and HCP.

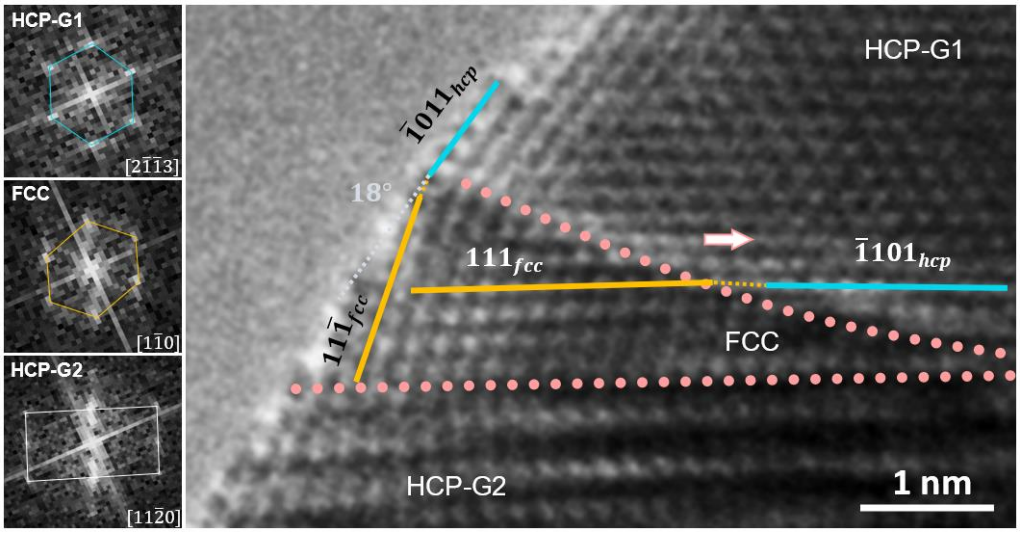

Fig. 7 Magnified HREM image of the FCC phase inside the new grain. The FFTs of the different regions are also shown. A unique lattice correspondence can be seen – the {111} of FCC is nearly parallel to the {$\bar{1}$101} of HCP matrix. The pink dotted lines denote the FCC/HCP phase boundaries. The solid lines are the corresponding planes of the FCC (in yellow) and the HCP matrix (in cyan).

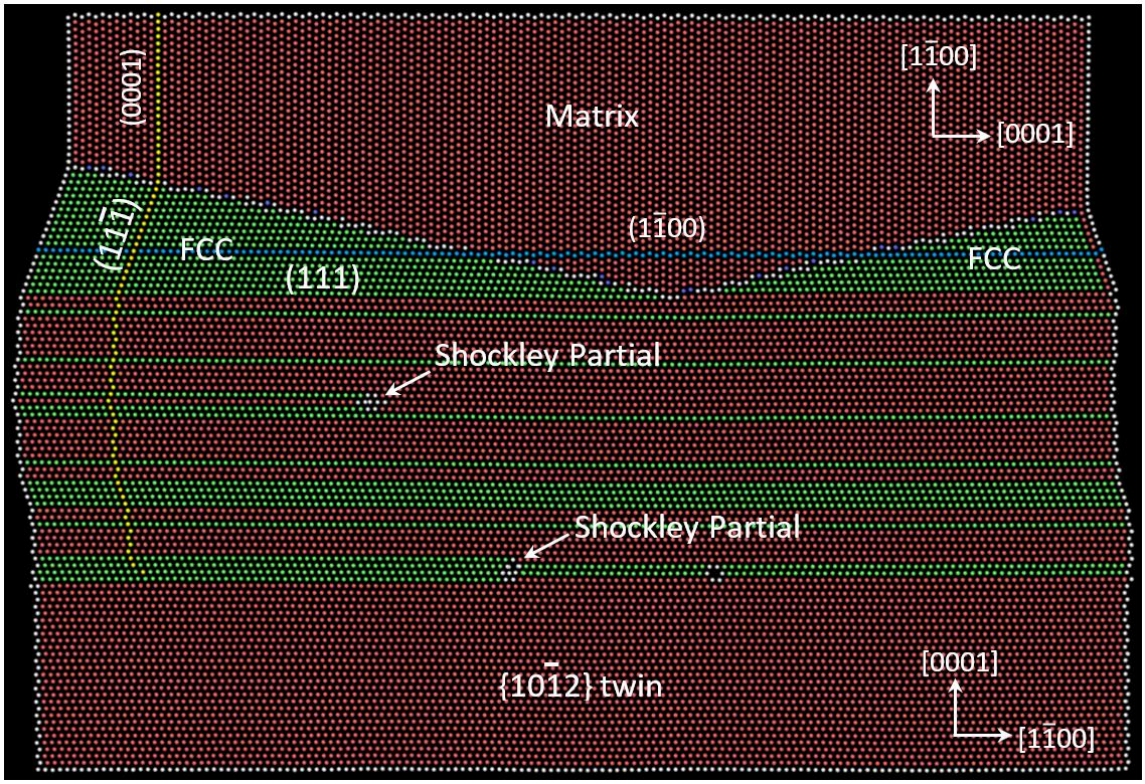

Fig. 8 Atomistic simulation result the bi-crystal satisfies $\{10\bar{1}2\}$ twin relationship. The common neighbor analysis is used to differentiate the structures, i.e., HCP in red, FCC in green. As the compressive strain increases, the bottom crystal grows upward into the matrix. An FCC phase is first formed in the two triangular regions. Residual FCC phase can also be seen in the $\{10\bar{1}2\}$ twin and is gradually transformed into the HCP twin by the Shockley partials. Note that the pre-selected prismatic plane of matrix is transformed into the (111) plane of FCC, and the (0001) of matrix into the $(11\bar{1})$ of FCC.

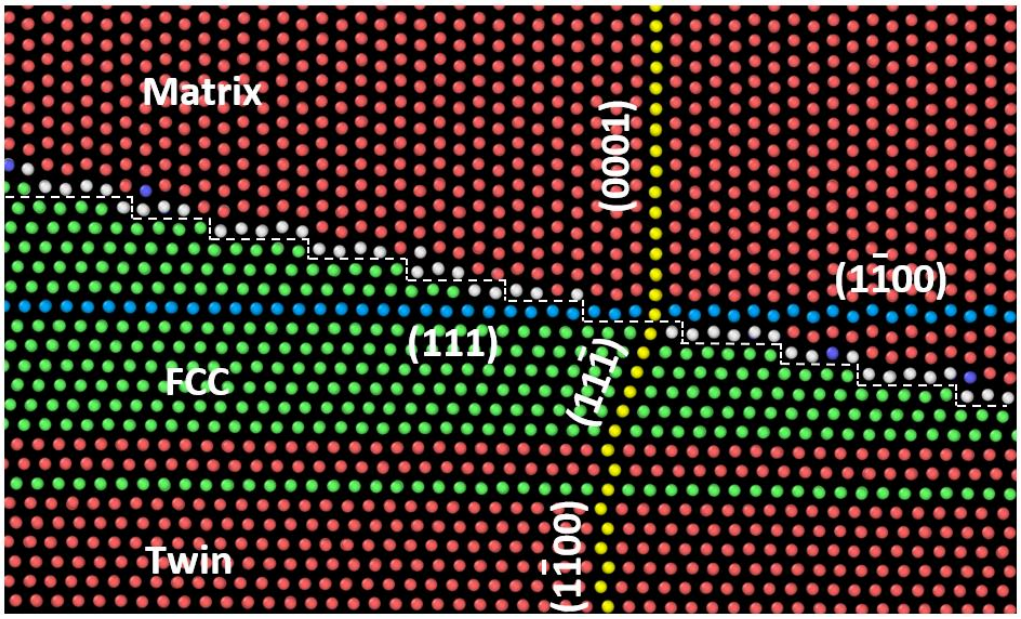

Fig. 9 A magnified view of the transformation of $(1\bar{1}00)_{matrix} \rightarrow (111)_{FCC}$, and $(11\bar{1})_{FCC} \rightarrow (1\bar{1}00)_{twin}$. The former lattice transformation is achieved by atomic shuffles that flatten the double-layered prismatic plane of matrix into the single-layered (111) plane of FCC, and an in-plane shear that produces the correct FCC stacking sequence. The latter lattice transformation is achieved by Shockley partial dislocations.

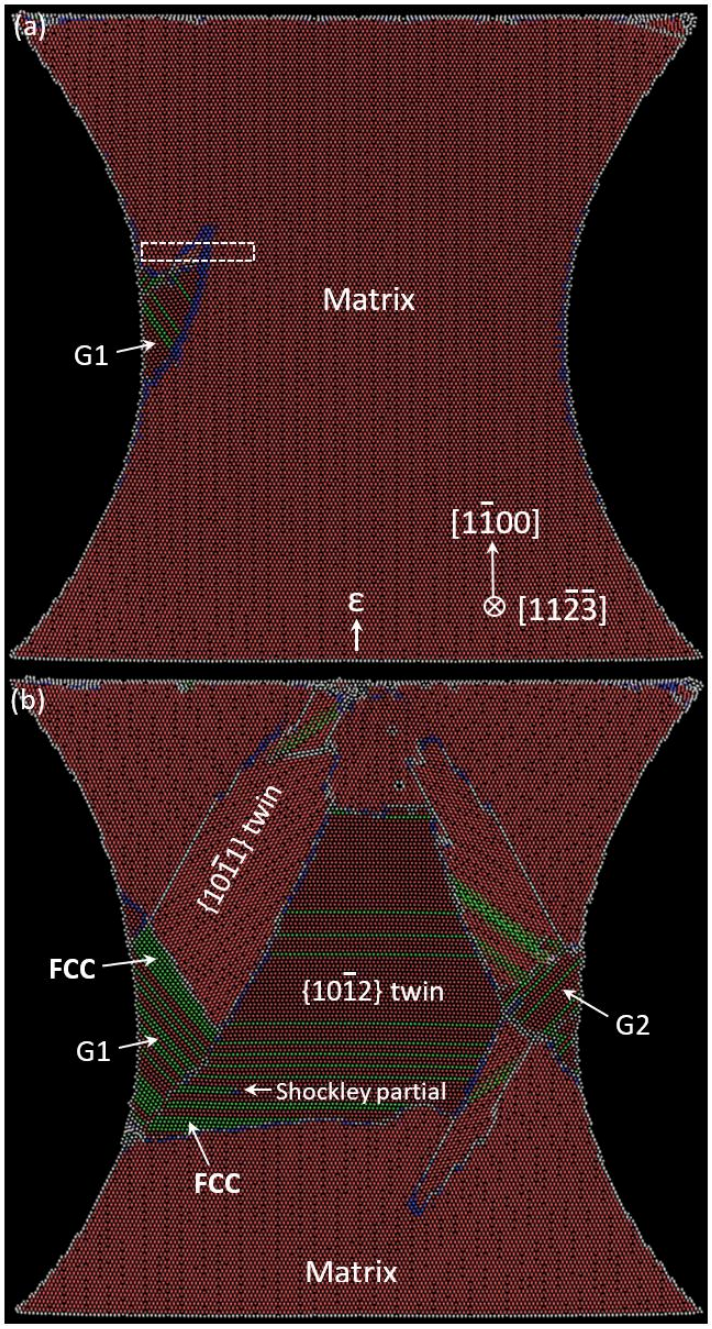

Fig. 10 (a) Uniaxial compression of the hour-glass shaped single crystal. A new grain (G1) is nucleated from the left surface. This new grain is not a twin. The boxed region is taken out for orientation relationship analysis. FCC structure has formed inside the G1. (b) As the compressive strain increases, another new grain G2 is formed. FCC structure can be seen inside G1 and G2. Meanwhile, $\{10\bar{1}2\}$ and $\{10\bar{1}1\}$ twins are also formed. FCC phase inside the $\{10\bar{1}2\}$ twin can be observed. As the $\{10\bar{1}2\}$ twin grows, the FCC phase is gradually transformed into the HCP twin by Shockley partials.

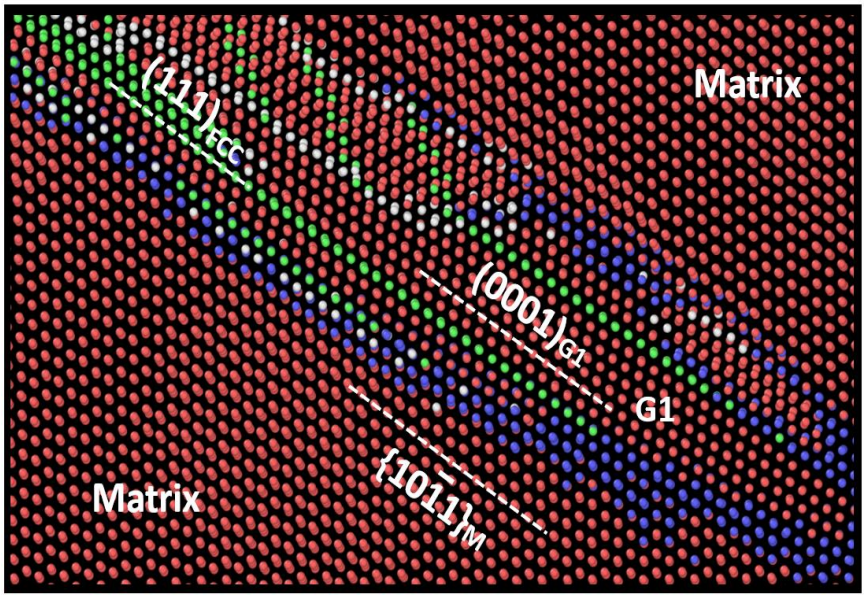

Fig. 11 Analysis of the orientation relationship (OR) between G1 and the matrix. The OR between the matrix and G1 satisfies: $(0001)_{G1} \parallel \{10\bar{1}1\}_M$, $\langle 10\bar{1}0\rangle_{G1} \parallel \langle 10\bar{1}2\rangle_M$. The OR between the FCC and G1 is: $(111)_{G1} \parallel (0001)_{G1}$, $[11\bar{2}]_{FCC} \parallel \langle 10\bar{1}0\rangle_{G1}$. The OR between the FCC and the matrix is: $(111)_{FCC} \parallel \{10\bar{1}1\}_M$, $[11\bar{2}]_{FCC} \parallel \langle 10\bar{1}2\rangle_M$.

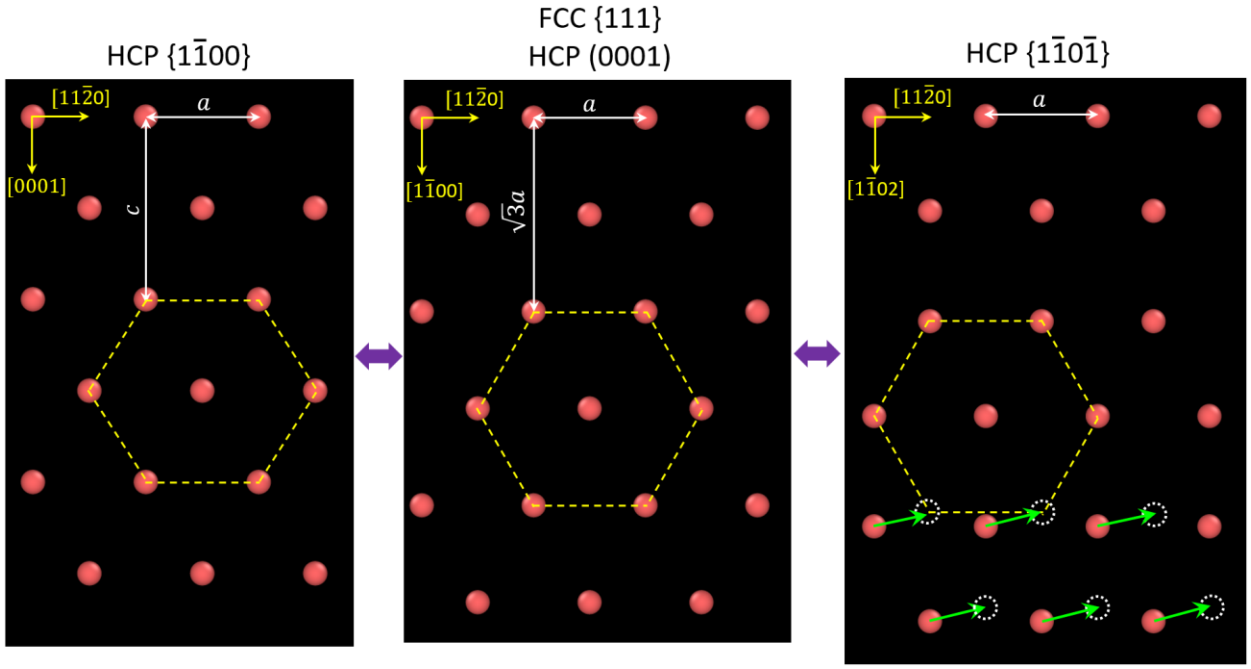

Fig. 12 Lattice transformations between basal (0001), prismatic {1$\bar{1}$00}, pyramidal {1$\bar{1}$0$\bar{1}$} of HCP. The planes are viewed along the respective plane normal and have the same magnification with respect to the lattice parameters. Note that (0001) and {1$\bar{1}$00} are a pair of corresponding planes of {10$\bar{1}$2} twinning mode, whereas (0001) and {1$\bar{1}$0$\bar{1}$} are a pair of corresponding planes of {10$\bar{1}$1} twinning mode. Because FCC {111} has the same structure as HCP (0001), an HCP {1$\bar{1}$00} and {1$\bar{1}$0$\bar{1}$} can be transformed into an FCC {111}, and vice versa. All these lattice transformations only involve atomic shuffles. Some of the large shuffles are denoted by the green arrows and the dotted circles.